Accepted Manuscript

Fabrication of Co/P25 coated with thin nitrogen-doped carbon shells (Co/P25/NC) as an efficient electrocatalyst for oxygen reduction reaction (ORR)

Koji Miyake, Toshiki Takemura, Atsushi Gabe, Yexin Zhu, Misaki Ota, Yasuhiro Shu, Yuichiro Hirota, Yoshiaki Uchida, Shunsuke Tanaka, Misaki Katayama, Yasuhiro Inada, Emilia Morallón, Diego Cazorla-Amorós, Norikazu Nishiyama

PII: S0013-4686(18)32553-2

DOI: https://doi.org/10.1016/j.electacta.2018.11.080

Reference: EA 33081

To appear in: *Electrochimica Acta*

Received Date: 9 October 2018

Accepted Date: 11 November 2018

Please cite this article as: K. Miyake, T. Takemura, A. Gabe, Y. Zhu, M. Ota, Y. Shu, Y. Hirota, Y. Uchida, S. Tanaka, M. Katayama, Y. Inada, E. Morallón, D. Cazorla-Amorós, N. Nishiyama, Fabrication of Co/P25 coated with thin nitrogen-doped carbon shells (Co/P25/NC) as an efficient electrocatalyst for oxygen reduction reaction (ORR), *Electrochimica Acta* (2018), doi: https://doi.org/10.1016/j.electacta.2018.11.080.

Fabrication of Co/P25 coated with thin Nitrogen-doped carbon shells (Co/P25/NC) as an efficient electrocatalyst for Oxygen Reduction Reaction (ORR)

Koji Miyake,*[a] Toshiki Takemura, [a] Atsushi Gabe,[b] Yexin Zhu,[a] Misaki Ota,[a] Yasuhiro Shu,[a] Yuichiro Hirota,[a] Yoshiaki Uchida,[a] Shunsuke Tanaka,[c] Misaki Katayama,[d] Yasuhiro Inada,[d] Emilia Morallón,[e] Diego Cazorla-Amorós [b] and Norikazu Nishiyama [a]

*a) Division of Chemical Engineering, Graduate School of Engineering Science, Osaka University, 1-3 Machikaneyama, Toyonaka, Osaka 560-8531, Japan. E-mail: *kojimiyake@cheng.es.osaka-u.ac.jp*

b) Departamento de Química Inorgánica and Instituto de Materiales. Universidad de Alicante, Ap. 99, 03080, Alicante, Spain.

c) Department of Chemical, Energy and Environmental Engineering, Kansai University, 3-3-35 Yamate, Suita, Japan.

d) Department of Applied Chemistry, Ritsumeikan University, 1-1-1 Noji-higashi, Kusatsu Shiga 525-8577, Japan

e) Departamento de Química Física and Instituto de Materiales. Universidad de Alicante, Ap. 99, 03080, Alicante, Spain.

Abstract

Development of electrocatalysts for oxygen reduction reaction (ORR) is important to solve the current problems about energy and fuel. As one of the catalysts with high performance, platina group metals (PGM) based catalysts have been widely known. However, PGM based catalysts are not suitable for large commercial application since the PGM based catalysts are so expensive. In this work, we have developed TiO_2 P25 coated with Co and nitrogen-doped carbon layers using commercially available and inexpensive P25 as a support (Co/P25/NC) as one of the alternatives to PGM based catalysts. Co/P25/NC showed an excellent catalytic activity on ORR compared to the other catalysts prepared using SiO_2, ZrO_2 and Al_2O_3 as a support. The ORR activity of Co/P25/NC was comparable to Pt based electrocatalysts. In addition, Co/P25/NC showed excellent durability and tolerance toward methanol compared to the Pt based catalyst. This work would provide a new synthetic strategy of electrocatalysts.

Keywords

P25 • Core-shell • CVD • CoNx • ORR

Introduction

High-efficient electrocatalytic processes are expected to solve some of the current problems of energy, fuel and environment. The reactions over electrocatalysts includes oxygen reduction reaction (ORR), hydrogen oxidation reaction (HOR), oxygen evolution reaction (OER) and hydrogen evolution reaction (HER). Platina group metals (PGMs) supported on carbon materials have been often used as electrocatalysts in these reactions due to their excellent catalytic performances. [1-8] However, PGMs are not suitable in large commercial applications since the cost of PGMs is so high. To overcome the disadvantage of PGMs, various electrocatalysts have been developed.

Bimetal catalysts of PGMs and non-PGMs have been developed to improve electrocatalytic performance with decreasing use of PGMs. [9-17] In particular, it was reported that Pt/Co or Pt/Ni based bimetal electrocatalysts show excellent catalytic performance on ORR due to electronic (alloying) effects. [10-12] One of the important factors that decide the performance of bimetal electrocatalysts is structure; e.g., core-shell structured bimetal electrocatalysts with PGMs as the shell show excellent catalytic performance with small amount of PGMs because active sites of PGMs can be effectively exposed besides alloying effect. [18-25] However, PGMs are still used even in these bimetal electrocatalysts. In this sense, non-PGMs electrocatalysts are more desirable.

Transition metals (Co, Fe, Ni, Mn and Cu) supported on carbon materials have been expected to be alternative electrocatalysts. [26-30] However, the electrocatalytic performances of only transition metals supported on carbon materials are still poor. Furthermore, these transition metals supported on carbon materials often show inferior electrocatalytic performance in acid media because these transition metals are dissolved in acid media. Recently, to improve the catalytic performances of the metal supported carbon materials, heteroatoms such as N, S and P were doped on those materials. [31-44] N coordinated Co or Fe (CoNx or FeNx) on the carbon materials can be excellent active sites for ORR. [40-44] In addition, electrocatalysts containing these sites show higher ORR durability in acid solution compared to that of transition metal oxides supported on carbon materials. [40, 42] However, it is difficult to create these sites precisely.

As another candidate, non-metals supported on carbon materials have been also fascinating recently. Heteroatoms (N, S, P and B) have been often doped into carbon structure to improve their electrocatalytic performances. [45-54] In particular, N-doped carbon materials have been widely known as a promising non-metal electrocatalyst. These non-metals supported on carbon materials can work even in acidic media. However, their catalytic activity is often lower than those of metals supported carbon materials.

In this work, we developed P25 (commercially available TiO_2) based electrocatalyst as a new candidate. Previously, we synthesized various core-shell structured materials. [54-65] In particular, we demonstrated that thin carbon shells (graphene) were deposited on P25 (commercially available and inexpensive TiO_2) by chemical vapour deposition (CVD) using methanol or propylene as carbon source. [65] In addition, we prepared Co nanoparticles modified carbon nanotubes with good ORR catalytic performance using poly vinyl pyrrolidone (PVP) as a protecting agent and $NaBH_4$ as a reduction agent. [31] Inspired by these findings, we fabricated P25 decorated with cobalt and N-doped carbon shells by combining the above methods. In this combined method, we expect that highly-dispersed CoNx species can be formed in the interface of TiO2/graphene. In addition, we also expect that CoNx species can be efficiently exposed to oxygen since CoNx is located in the shell layer, leading to higher catalytic performance. As comparison, we also used other supports such as SiO_2, Al_2O_3 and ZrO_2. The prepared samples were characterized by X-ray diffraction (XRD), X-ray Photoelectron Spectroscopy (XPS), Thermo Gravimetry (TG), X-ray absorption fine structure (XAFS), and Transmission Electron Microscopy (TEM) and the electrocatalytic properties were evaluated.

Experimental

1. Materials

We used P25 (Degussa), SiO_2, Al_2O_3 and ZrO_2 as supports. SiO_2 and ZrO_2 supports were obtained from colloidal silica solution (Aldrich) or zirconia solution (Nissan Chemical Industries) by drying at 363 K. As for Al_2O_3, alumina solution (KAWAKEN Fine Chemicals) was dried at 363 K, and calcined at 773 K for 9 h to remove the impurities. Cobalt Nitrate (Wako), poly vinyl pyrrolidone (PVP, Wako), $NaBH_4$ (Wako) and ethanol (Wako) were used as cobalt source, a protecting agent, a reduction agent and solution. Acetonitrile was used as carbon and nitrogen sources for chemical vapour deposition (CVD)

2. Preparation of Co/P25/NC

Firstly, we prepared 1 wt% Co supported P25. Typically, cobalt nitrate and PVP were dissolved in ethanol, and P25 was added into the solution. The mixture was cooled in an iced bath, and $NaBH_4$ was added dropwise. The mixture was stirred at 273 K for 2 h, and the solution was evaporated at 363 K. To remove PVP, the obtained powders were calcined at 773 K for 3 h under nitrogen atmosphere.

Next, we carried out CVD using acetonitrile as carbon and nitrogen sources to coat N-doped carbon layers on the prepared supports. Acetonitrile vapour was fed by a saturator. The treatment temperature and time were 773 K and 1 h, respectively. Finally, the carbonization was carried out under nitrogen atmosphere at 973 K for 3 h. The obtained sample was named as Co/P25/NC.

In order to investigate the effect of supports, we synthesized other catalysts using other supports such as SiO_2, Al_2O_3 and ZrO_2. Those samples were named as $Co/SiO_2/NC$, $Co/Al_2O_3/NC$ and $Co/ZrO_2/NC$, respectively. In addition, we also investigated the effect of the crystalline state of TiO_2 toward ORR activity. We prepared different TiO_2 based catalysts using anatase or rutile phase TiO_2. The samples were named as Co/a-TiO_2/NC and Co/r-TiO_2/NC, respectively.

3. Characterization

The crystal structures of the prepared samples were determined by X-ray diffraction (XRD) recorded on the PANalytical X'Pert-MPD diffractometer using Cu-Kα radiation. Transmission electron microscopy (TEM) images were recorded. The amount of deposited nitrogen-doped carbon was estimated by Thermo Gravimetry (TG) analyser. The chemical states were characterized by X-ray Photoelectron Spectroscopy (XPS) using a JPS-9000MX spectrometer (JEOL) with Mg Kα source radiation (10 kV, 10 mA) as the energy source. The X-ray absorption fine structure (XAFS) measurement was performed at BL-3 of the Ritsumeikan Synchrotron Radiation Center (Japan) using

a Si(220) double crystal monochromator. The Co K edge XAFS spectra were measured in fluorescence yield mode using a scintillation counter.

4. Electrochemical characterization

Electrochemical activity tests towards ORR were carried out at 298 K in a three-electrode cell with 0.1M KOH electrolyte using an Autolab PGSTAT302 (Metrohm, Netherlands) potentiostat, a Pt wire as counter electrode and Reversible Hydrogen Electrode (RHE) as reference electrode. A rotating ring-disk electrode (RRDE, Pine Research Instruments, USA) equipped with a glassy carbon (GC) disk (5.61 mm diameter) and an attached Pt ring was used as working electrode. The samples were dispersed in a solution of 20 vol.% of isopropanol, 80 vol.% of water and 0.02 vol.% of Nafion@ to prepare a final dispersion of 1mg/ml of the prepared catalysts. And then, 100 µl (mass of electrode is 400 µg/cm^2) of the dispersion was pipetted on a GC electrode to obtain uniform catalysts layer for ORR study. The sample on the GC was dried by heating lamp for evaporation of the solvent. Cyclic Voltammetry (CV) and linear sweep voltammetry (LSV) from 1 to 0 V were carried out. The CV was performed in N_2 saturated atmosphere at 5 and 50 mV/s. The LSV was done in an O_2-saturated atmosphere for different rotation rates between 400 and 2025 rpm at 5 mV/s. The potential of the ring was kept at 1.5V and the ring current by H_2O_2 oxidation was also measured during the LSV measurement. The electron transfer number (n) of ORR on the catalysts modified electrode was determined by the following equation [66].

$$n=(4\times I_d)/(I_d+I_r/N)$$

where I_d is disk current, I_r is ring current, and N is the collection efficiency of the ring which was experimentally determined to be 0.37.

Results and discussion

Fig. 1 shows the XRD patterns of X and Co/X/NC samples, where X= P25, SiO_2, Al_2O_3 and ZrO_2. The specific peak around 25 degrees was detected in XRD patterns of P25 and Co/P25/NC. This specific peak is derived from anatase phase. However, a peak at around 27 degrees which is derived from rutile phase was also found. Therefore, although P25 and Co/P25/NC have mainly anatase phase, rutile phase is also included as impurity. The intensity of Co/P25/NC at around 27 degrees was higher compared to P25, suggesting that some anatase phase changed into rutile phase during the thermal treatments such as removal of PVP, CVD or carbonization. There is only a broad peak in the XRD pattern of SiO_2, indicating that SiO_2 has amorphous phase. Meanwhile, in the XRD pattern of Co/SiO_2/NC, a specific peak was observed around 22 degrees. This result shows that crystalline structure of SiO_2 was transformed during some thermal

treatments such as removal of PVP, CVD or carbonization. As for Al_2O_3 and ZrO_2 based samples, there are no changes in their XRD patterns. This is because Al_2O_3 and ZrO_2 supports are thermally stable under our treatment conditions. However, there are no peaks derived from cobalt species in XRD patterns of Co/X/NC even though the presence of Co species was confirmed by XPS as shown below. This result suggests that large particles (larger than a few nm) were not formed. In addition, there are no broad peaks derived from carbon in XRD patterns of Co/X/NC, indicating that the deposited carbon layers are very thin.

The TEM images for prepared catalysts are shown in Fig. 2. Cobalt nanoparticles were clearly observed in the TEM images of $Co/Al_2O_3/NC$. Meanwhile, as for the others, cobalt nanoparticles were not observed, exhibiting that Co/P25/NC, Co/SiO_2 /NC and Co/ZrO_2/NC have very small Co species (smaller than 1 nm). These results also suggest that highly dispersed cobalt species could be favourably formed on P25, SiO_2 and ZrO_2 using PVP as a protecting agent and $NaBH_4$ as a reduction agent.

We estimated the deposition amount of N-doped carbon on the supports using TG analysis. The deposition amounts of N-doped carbon on Co/P25/NC, Co/SiO_2 /NC, Co/Al_2O_3/NC and Co/ZrO_2/NC were 3.2 wt%, 0.3 wt%, 5.7 wt% and 6.9 wt%, respectively. These results exhibit that N-doped carbon cannot be formed on SiO_2 by CVD at 773 K using acetonitrile vapour. This result indicates that the surface of TiO_2, Al_2O_3 and ZrO_2 shows catalytic activity for dehydrogenation and aromatization of acetonitrile.

Fig 3 shows XPS spectra of Co 2P and N 1s. Signals derived from Co species were detected in all samples. However, the intensity of Co/P25/NC was much lower compared to the other samples although the amount of Co was similar in all samples. This result suggested that Co species of Co/P25/NC were well covered with carbon layers. Meanwhile, signals derived from N were detected in all samples, indicating N-doped carbon layers were successfully formed in our method. However, the intensity of the signals on Co/SiO_2/NC was lower than those on the other samples. This is because the amount of N-doped carbon on Co/SiO_2/NC was much lower compared to the other samples. In addition, the intensity on Co/Al_2O_3/NC was lower than those on Co/P25/NC and Co/ZrO_2/NC although the amount of carbon on Co/Al_2O_3/NC was enough high, indicating that P25 and ZrO_2 are good catalysts to facilitate the formation of carbon layers with high content of N. The spectra of all samples could be deconvoluted into three peaks derived from pyridinic N (around 398 eV), pyrrolic/pyridonic N (around 399 eV) and quaternary N (around 401eV), respectively.[31]

We also performed Co K-edge XANES measurements to investigate the chemical state of Co species in more detail. Co K-edge XANES spectra were shown in Fig 4. The Co K-edge XANES spectra of Co/P25/NC and Co/ZrO_2/NC were different from those of Co/SiO_2/NC and Co/Al_2O_3/NC. The Co K-edge XANES spectra of Co/P25/NC and Co/ZrO_2/NC were similar to those of carbons with CoNx species, [43, 67, 68] suggesting thatCo/P25/NC and Co/ZrO_2/NC have CoNx species.

The CV curves for Co/P25/NC, Co/SiO_2/NC, Co/Al_2O_3/NC and Co/ZrO_2/NC are shown in Fig. 5(a). The gravimetric capacitances of Co/P25/NC, Co/SiO_2/NC, Co/Al_2O_3/NC and Co/ZrO_2/NC are 10.2, 0.8, 3.2 and 10.7 F/g, respectively. The amount of N-doped carbon for Co/SiO_2/NC was much lower compared to the other samples, leading to low conductivity. Co/Al_2O_3/NC showed a lower capacitance than Co/P25/NC and Co/ZrO_2/NC despite the amount of N-doped carbon on Co/Al_2O_3/NC is higher than in the case of Co/SiO_2/NC sample. One possible reason is that N content of Co/Al_2O_3/NC was lower than those of Co/P25/NC and Co/ZrO_2/NC. The other possible reason is that larger particle size that produces a lower electroactive surface area decreasing the capacitance. The LSV curves are shown in Fig. 5(b). Co/P25/NC showed the most superior catalytic performance for ORR. Meanwhile, Co/SiO_2/NC showed the most inferior catalytic performance. This is because the deposition amount of N-doped carbons was very small, which results in very low conductivity. Meanwhile, Co/Al_2O_3/NC showed inferior catalytic performance compared to Co/P25/NC and Co/ZrO_2/NC although the content of N-doped carbon was high. Several groups reported that CoNx species are effective active sites for ORR. [31, 40-44] Co/Al_2O_3/NC had larger cobalt nanoparticles than Co/P25/NC and Co/ZrO_2/NC. Due to this, the amount of CoNx on Co/Al_2O_3/NC was smaller than those on Co/P25/NC and Co/ZrO_2/NC. In addition, the conductivity of Co/Al_2O_3/NC was lower compared to Co/P25/NC and Co/ZrO_2/NC. This low amount of CoNx and low conductivity of Co/Al_2O_3/NC would lead to the inferior catalytic performance compared to Co/P25/NC and Co/ZrO_2/NC. Although Co/ZrO_2/NC had CoNx species like Co/P25/NC, Co/ZrO_2/NC showed inferior catalytic performance to Co/P25/NC. In the TEM images of Co/ZrO_2/NC, large cobalt species were not observed. However, intensity of Co/ZrO_2/NC on Co 2p was stronger compared to Co/P25/NC. The results indicate that Co species on ZrO_2 were not completely covered with N-doped carbon. These uncovered cobalt species cannot act as efficient active sites for ORR. Meanwhile, covered cobalt species would be CoNx species on carbon which are proposed as active sites for ORR. Thus, although N-doped carbon layers were almost completely deposited on cobalt species of Co/P25 by CVD, N-doped carbon layers were not completely deposited on cobalt species of Co/ZrO_2 by

CVD. Owing to this, Co/ZrO_2/NC showed inferior catalytic performance on ORR to Co/P25/NC.

In order to investigate the effect of crystal structure of TiO_2 on ORR, we prepared Co/a-TiO2/NC and Co/r-TiO_2/NC using TiO_2 with anatase or rutile phase, respectively. LSV curves of Co/a-TiO_2/NC and Co/r-TiO2/NC are shown in Fig. 6. Co/a-TiO_2/NC showed better catalytic performance than Co/r-TiO_2/NC. From the TEM images (Fig. S1), it was confirmed that Co/r-TiO_2/NC had larger cobalt nanoparticles than Co/a-TiO_2/NC, exhibiting that highly dispersed cobalt species were formed on TiO_2 with anatase phase. Furthermore, the conductivity of Co/a-TiO_2/NC was higher than Co/r-TiO_2/NC. This result indicates that N-doped carbon layers with high conductivity were favourably formed on TiO_2 with anatase phase. In short, anatase phase of TiO_2 contributed to the formation of highly dispersed cobalt species and N-doped carbon layers with high conductivity on the support.

LSV curves over Co/P25/NC and Pt-based catalysts are shown in Fig. 7. The catalytic performance of Co/P25/NC with 400 $\mu g_{cat}/cm^2$ was worse than that of commercial 20 wt% Pt/C with 400 $\mu g_{cat}/cm^2$. This is because 20 wt% Pt/C has high content of Pt. However, high loading of Pt disturbs the commercial application in terms of cost because the cost of Pt-based catalyst is controlled by the amount of Pt. Decreasing the amount of Pt is so desirable. Actually, in some papers, LSV curves of 20 wt% Pt/C with smaller amount of catalyst on the disk were applied as reference compared to those of non-PGM catalysts on the disk. [38, 40, 44] So, we discussed the catalytic property based on the amount of metals on the disk in order to investigate the efficiency of loaded metals. The current density of Co/P25/NC and 20wt% Pt/C with different amounts of catalyst on the disk at 0.65 V are summarized in Table 1. The current density of Co/P25/NC with 400 $\mu g_{cat}/cm^2$ (3 $\mu g_{Co}/cm^2$) at 0.65 V was better than that of 20 wt% Pt/C with 50 and 25 $\mu g_{cat}/cm^2$ (10 and 5 $\mu g_{Pt}/cm^2$, respectively), although Co content on the disk was lower than Pt content on the disk in these conditions. We also investigated the catalytic performance of commercial Pt/C containing similar amount of loaded metals (1 wt%) with Co/P25/NC because there is a possibility that the high loading of Pt makes the efficiency of Pt decreased. The catalytic performance of Co/P25/NC with 400 $\mu g_{cat}/cm^2$ (3 $\mu g_{Co}/cm^2$) was better than that of commercial 1 wt% Pt/C with 400 $\mu g_{cat}/cm^2$ (4 $\mu g_{Pt}/cm^2$) despite that the Co content on the disk was lower than Pt content on the disk Pt/C even in this condition. Hence, these results indicate that Co species of Co/P25/NC is an efficient active site for ORR.

We also investigated the durability and methanol tolerance of Co/P25/NC. The durability test was conducted by RDE chronoamperometry under steady state mass

transport conditions (0.65 V vs. RHE). As for the methanol tolerance. We added 1M methanol after 120 min reaction. The results are shown in Fig. 8. The relative current density of 20 wt% Pt/C decreased to 89 % after 120 min. After adding methanol, the current density of 20 wt% Pt/C dramatically dropped down. This is because methanol decomposes on Pt forming adsorbed CO poisoning the Pt surface [1]. Meanwhile, Co/P25/NC showed higher relative current density (94 %) after 120 min compared to 20 wt% Pt/C. In addition, significant decrease of the current density of Co/P25/NC was not observed after adding methanol. The result showed that Co/P25/NC is a suitable catalyst in terms of durability and methanol tolerance.

Conclusion

We have successfully synthesized P25 coated with Co and nitrogen-doped carbon layers (Co/P25/NC). Some characterizations suggested that Co/P25/NC had sufficient CoNx species compared to other samples prepared using SiO_2, Al_2O_3 and ZrO_2 as supports. It was found that P25 was the best support to achieve the formation of CoNx in the shell layers. Thanks to the presence of CoNx species in Co/P25/NC, Co/P25/NC showed excellent catalytic performance for ORR. The current density of Co/P25/NC at 0.65 V vs. RHE was better than that of 1 wt% Pt/C and comparable to that of 20 wt% Pt/C despite the Co content of Co/P25/NC was very small, indicating that Co/P25/NC has efficient metal active sites for ORR. In addition, Co/P25/NC showed better durability than 20 wt% Pt/C, and methanol tolerance of Co/P25/NC was much better than that of 20 wt% Pt/C. This work provides a new insight for designing of electrocatalysts.

Acknowledgements

We would like to thank the GHAS laboratory at Osaka University for the XRD measurements. The TEM measurement was carried out by using a facility in the Research Center for Ultrahigh Voltage Electron Microscopy, Osaka University. The financial support by MINECO (CTQ2015-66080-R) and HEIWA NAKAJIMA FOUNDATION is acknowledged.

References

[1] E. Morallón, A. Rodes, J.L. Vázquez, J.M. Pérez, *J. Electroanalytical Chemistry*, 1995, **391**, 149-157.

[2] F. H. B. Lima, J. Zhang, M. H. Shao, K. Sasaki, M. B. Vukmirovic, E. A. Ticianelli, and R. R. Adzic *J. Phys. Chem. C*, 2007, **111**, 404-410.

[3] H. Ataee-Esfahani, L. Wang, Yoshihiro Nemoto and Yusuke Yamauchi, *Chem. Mater.*, 2010, **22**, 6310–6318.

[4] R. Choi, S. Choi, C. H. Choi, K. M. Nam, S. Woo, J. T. Park and Sang Woo Han, *Chem. Eur. J.*, 2013, **19**, 8190 – 8198.

[5] T. Reier, M. Oezaslan and P. Strasser, *ACS Catal.*, 2012, **2**, 1765–1772.

[6] T. Zhang, S.-C. Li, W. Zhu, Z.-P. Zhang, J. Gua and Y.-W. Zhang, *Nanoscale*, 2017,**9**, 1154-1165.

[7] J. Ohyama, D. Kumadaa and A. Satsuma, *J. Mater. Chem. A*, 2016, **4**, 15980-15985.

[8] E. Kemppainen, A. Bodin, B. Sebok, T. Pedersen, B. Seger, B. Mei, D. Bae, P. C. K.

[9] Vesborg, J. Halme, O. Hansen, P. D. Lund and I. Chorkendorff, *Energy Environ. Sci.*, 2015, **8**, 2991-2999.

[10] W. Chen, J. Kim, S. Sun and S. Chen, *J. Phys. Chem. C*, 2008, **112**, 3891-3898.

J. Wu, A. Gross and H. Yang, *Nano Lett.*, 2011, **11**, 798–802.

[11] C. Wang, M. Chi, G. Wang, D. van der Vliet, D. Li, K. More, H. Wang, J. A. Schlueter, N. M. Markovic, *Adv. Funct. Mater.*, 2011, **21**, 147–152.

[12] C. Wang, M. Chi, D. Li, D. van der Vliet, G. Wang, Q. Lin, J. F. Mitchell, K. L. More, N. M. Markovic and V. R. Stamenkovic and V. R. Stamenkovic, *ACS Catal.*, 2011, **1**, 1355–1359.

[13] S. M. Alia, S. Shulda, C. Ngo, S. Pylypenko and B. S. Pivovar, *ACS Catal.*, 2018, **8**, 2111–2120.

[14] J. Lim, S. Yang, C. Kim, C.-W. Roh, Y. Kwon, Y.-T. Kim and H. Lee, *Chem. Commun.*, 2016, **52**, 5641-5644.

[15] X. Y. Xu, X. F. Dong, Z. J. Bao, R. Wang, J. G. Hu and H. B. Zeng, *J. Mater. Chem. A*, 2017,**5**, 22654-22661.

[16] G. Y. Shi, H. Yano, D. A. Tryk, M. Watanabe, A. Iiyama and H. Uchida, *Nanoscale*, 2016, **8**, 13893-13897.

[17] G. Shi, H. Yano, D. A. Tryk, M. Matsumoto, H. Tanida, M. Arao, H. Imai, J. Inukai, A. Iiyama and H. Uchida, *Catal. Sci. Technol.*, 2017, **7**, 6124-6131.

[18] P. Mani, R. Srivastava and P. Strasser, *J. Phys. Chem. C*, 2008, **112**, 2770-2778.

[19] Z. Liu, G. S. Jackson, and B. W. Eichhorn, *Angew. Chem. Int. Ed.*, 2010, **49**, 3173 – 3176.

[20] G. Hu, E. Gracia-Espino, R. Sandström, T. Sharifi, S. Cheng, H. Shen, C. Wang, S. Guo, G. Yang and T. Wågberg, *Catal. Sci. Technol.*, 2016, **6**, 1393.

[21] Y. Xiong, L. Xiao, Y. Yang, F. J. DiSalvo, and Héctor D. Abruña, *Chem. Mater.*, 2018, **30**, 1532−1539.

[22] H. N. Nong, L. Gan, E. Willinger, D. Teschner and P. Strasser, *Chem. Sci.*, 2014, **5**,

2955-2963.
[23] S. Park, D. Yoon, S. Bang, J. Kim, H. Baik, H. Yang and K. Lee, *Nanoscale*, 2015, **7**, 15065-15069.
[24] H. Lv, Z. Xi, Z. Chen, S. Guo, Y. Yu, W. Zhu, Q. Li, X. Zhang, M. Pan, G. Lu, S. Mu and S. Sun, *J. Am. Chem. Soc.*, 2015, **137**, 5859–5862.
[25] M. Wang, J. Huang, M. Wang, D. Zhang, W. Zhang, W. Li and J. Chen, *Electrochemistry Communications*, 2013, **34**, 299–303.
[26] K. N. Zhu, H. Y. Qin, B. H. Liu, Z. P. Li, *Journal of Power Sources*, 2011, **196**, 182–185.
[27] S. N.S. Goubert-Renaudin, A. Wieckowski, *Journal of Electroanalytical Chemistry*, 2011 **652**, 44–51.
[28] H. Zhang, Z. Zhang, N. Li, W. Yan, Z. Zhu, *J. Catal.*, 2017, **352**, 239–245.
[29] F. Cheng, Y. Su, J. Liang, Z. Tao, and J. Chen, *Chem. Mater.*, 2010, **22**, 898–905
[30] P. Hosseini-Benhangi, C. H. Kung, A. Alfantazi and E. L. Gyenge, *ACS Appl. Mater. Interfaces*, 2017, **9**, 26771−26785.
[31] A. Gabe, J. García-Aguilar, Á. Berenguer-Murcia, E. Morallón and D. Cazorla-Amorós, *Applied Catalysis B: Environmental*, 2017, **217**, 303–312.
[32] X. Fu, J. Choi, P. Zamani, G. Jiang, Md. A. Hoque, F. M. Hassan and Z. Chen, *ACS Appl. Mater. Interfaces*, 2016, **8**, 6488−6495.
[33] C. González-Gaitán, R. Ruiz-Rosas, E. Morallón and D. Cazorla-Amorós, *Langmuir*, 2017, **33**, 11945−11955.
[34] Y. Jiang, Y. Lu, X. Lv, D. Han, Q. Zhang, L. Niu and W. Chen, *ACS Catal.*, 2013, **3**, 1263−1271.
[35] Z. Zhen, Z. Jiang, X. Tian, L. Zhou, B. Deng, B. Chen and Z.-J. Jiang, *RSC Adv.*, 2018, **8**, 14462.
[36] R. Zhang, S. He, Y. Lu and W. Chen, *J. Mater. Chem. A,* 2015, **3,** 3559.
[37] L. Zhu, D. Susac, M. Teo, K.C. Wong, P.C. Wong, R.R. Parsons, D. Bizzotto K.A.R. Mitchell, S.A. Campbell, *J. Catal.*, 2008, **258**, 235–242.
[38] M. Wu, Q. Tang, F. Dong, Z. Bai, L. Zhang, J. Qiao, *J. Catal.*, 2017, **352**, 208–217.
[39] S. N.S. Goubert-Renaudin, X. Zhu, A. Wieckowski, *Electrochemistry Communications*, 2010, **12**, 1457–1461.
[40] X. X. Wang, D. A. Cullen, Y.-T. Pan, S. Hwang, M. Wang, Z. Feng, J. Wang, M. H. Engelhard, H. Zhang, Y. He, Y. Shao, D. Su, K. L. More, J. S. Spendelow and G. Wu, *Adv. Mater.*, 2018, **30**, 1706758.
[41] U. I. Kramm, I. Herrmann-Geppert, J. Behrends, K. Lips, S. Fiechter and P. Bogdanoff, *J. Am. Chem. Soc.*, 2016, **138**, 635–640.

[42] H. Zhang, S. Hwang, M. Wang, Z. Feng, S. Karakalos, L. Luo, Z. Qiao, X. Xie, C. Wang, D. Su, Y. Shao and G. Wu, *J. Am. Chem. Soc.*, 2017, **139**, 14143–14149.

[43] T. He, H. Xue, X. Wang, S. He, Y. Lei, Y. Zhang, R. Shen, Y. Zhang and J. Xiang, *Nanoscale*, 2017, **9**, 8341-8348.

[44] P. Yin, T. Yao, Y. Wu, L. Zheng, Y. Lin, W. Liu, H. Ju, J. Zhu, X. Hong, Z. Deng, G. Zhou, S. Wei, Y. Li, *Angew. Chem. Int.*, 2016, **55**, 10800-10805.

[45] C. He, Z. Li, M. Cai, M.i Cai, J.-Q. Wang, Z. Tian, X. Zhang and P. K. Shen, *J. Mater. Chem. A*, 2013, **1**, 1401.

[46] J. Quílez-Bermejo, C. González-Gaitán b, E. Morallón and D. Cazorla-Amorós, *Carbon*, 2017, **119**, 62-71.

[47] X. Zhu, Y. Zhu, C. Tian, T. Jin, X. Yang, X. Jin, C. Li, H. Wang, H. Liu and S. Dai, *J. Mater. Chem. A*, 2017, **5**, 4507.

[48] T. Zhou, R. Ma, Y. Zhou, R. Xing, Qian Liu, Y. Zhu, J. Wang, *Microporous and Mesoporous Materials*, 2018, **261**, 88–97.

[49] C. You, X. Jiang, L. Han X. Wang, Q. Lin, Y. Hu, C. Wang, X. Liu and S. Liao, *J. Mater. Chem. A*, 2017, **5**, 1742.

[50] L. Qin, L. Wang, X. Yang, R. Ding, Z. Zheng, X. Chen, B. Lv, *J. Catal.*, 2018, **359**, 242–250.

[51] C. H. Choi, M. W. Chung, H. C. Kwon, S. H. Park and S. I. Woo, *J. Mater. Chem. A*, 2013, **1**, 3694.

[52] G. Zhuang, J. Bai, X. Tao, J. Luo, X. Zhou, W. Chen, X. Zhong, X. Li and J. Wang, *Microporous and Mesoporous Materials*, 2018, **256**, 75-83.

[53] S. Liu, G. Li, Y. Gao, Z. Xiao, J. Zhang, Q. Wang, X. Zhang and L. Wang, *Catal. Sci. Technol.*, 2017, **7**, 4007.

[54] Norikazu Nishiyama, Manabu Miyamoto, Yasuyuki Egashira, Korekazu Ueyama, *Chem. Commun*., 2001, 1746-1747.

[55] N. Nishiyama, K. Ichioka, M. Miyamoto, Y. Egashira, K. Ueyama, L. Gora, W. Zhu, F. Kapteijn, J. A. Moulijn, *Microporous and Mesoporous Materials*, 2005, **83**, 244-250.

[56] M. Miyamoto, T. Kamei, N. Nishiyama, Y. Egashira, K. Ueyama, *Adv. Mater.*, 2005, **17**, 1985-1988.

[57] D. V. Vu, M. Miyamoto, N. Nishiyama, Y. Egashira, K. Ueyama, J. Catal., 2006, **243**, 389-394.

[58] D. V. Vu, M. Miyamoto, N. Nishiyama, S. Ichikawa, Y. Egashira, K. Ueyama, *Microporous and Mesoporous Materials*, 2008, **115**, 106-112.

[59] D. V. Vu, M. Miyamoto, N. Nishiyama, Y. Egashira, K. Ueyama, *Catal. Lett.*, 2009 **127**, 233-238.

[60] Y. Sugiura, Y. Hirota, Y. Uchida, N. Nishiyama, *Chem. Lett.*, 2015, **44**, 477-479.
[61] M. Miyamoto, K. Mabuchi, J. Kamada, Y. Hirota, Y. Oumi, N. Nishiyama, S. Uemiya, *J. Por. Mater.*, 2015 **22**, 769-778.
[62] K. Miyake, Y. Hirota, K. Ono, Y. Uchida, N. Nishiyama, *ChemistrySelect*, 2016, **1**, 967-969.
[63] K. Miyake, Y. Hirota, K. Ono, Y. Uchida, S. Tanaka, N. Nishiyama, *J. Catal.*, 2016, **342**, 63-66.
[64] K. Miyake, R. Inoue, M. Nakai, Y. Hirota, Y. Uchida, S. Tanaka, M. Miyamoto, N. Nishiyama, *Microporous and Mesoporous Materials*, 2018, **271**, 156-159.
[65] M. A. Fitri, M. Ota, Y. Hirota, Y. Uchida, K. Hara, D. Ino, N. Nishiyama, *Materials Chemistry and Physics*, 2017, **198**, 42-48.
[66] U.A. Paulus, T.J. Schmidt, H.A. Gasteiger, R.J. Behm, *J. Electroanal. Chem.*, 2011, **495**, 134–145.
[67] J. Xie, J.D. Kammert, N. Kaylor, J. W. Zheng, E. Choi, H. N. Pham, X. Sang, E. Stavitski, K. Attenkofer, R. R. Unocic, A. K. Datye and R. J. Davis, *ACS Catal.*, 2018, **8**, 3875−3884.
[68] X. Sun, A. I. Olivos-Suarez, .i Osadchii, M. J. Valero Romero, F. Kapteijn and Jorge Gascon, *J. Catal.*, 2018, **357**, 20-28.

Figure and Table captions

Fig. 1 XRD patterns of (a) P25 based samples, (b) SiO_2 based samples, (c) Al_2O_3 based samples and (d) ZrO_2 based samples.

Fig. 2 TEM images of (a) P25 based samples, (b) SiO_2 based samples, (c) Al_2O_3 based samples and (d) ZrO_2 based samples.

Fig. 3 XPS spectra of Co/P25/NC, Co/SiO_2/NC, Co/Al_2O_3/NC and Co/ZrO_2 /NC on (a) Co 2p and (b) N 1s.

Fig. 4 Co K edge XANES spectra of Co/P25/NC, Co/SiO_2/NC, Co/Al_2O_3/NC and Co/ZrO_2 /NC.

Fig. 5 (a) Steady state voltammograms in N_2-saturated 0.1 M KOH with a scan rate of 50 mV/s, (b) LSV curves and (c) electron transfer number during ORR in O_2-saturated 0.1 M KOH at 1600 rpm with a sweep rate of 5 mV/s over Co/P25/NC, Co/SiO_2/NC, Co/Al_2O_3/NC and Co/ZrO_2 /NC.

Fig. 6 LSV curves in O_2-saturated 0.1 M KOH at 1600 rpm with a sweep rate of 5 mV/s over Co/a-TiO_2/NC and Co/r-TiO_2/NC.

Fig. 7 LSV curves in O_2-saturated 0.1 M KOH at 1600 rpm with a sweep rate of 5 mV/s over Co/P25/NC, 1 wt% Pt/C and 20 wt% Pt/C with different amounts of catalysts.

Fig. 8 Relative current density versus time over Co/P25/NC and 20 wt% Pt/C. (After 120 min, 1M methanol injected).

Table 1 Summary of current density @ 0.65 V vs. RHE over Co/P25/NC, 20 wt% Pt/C and 1 wt% Pt/C.

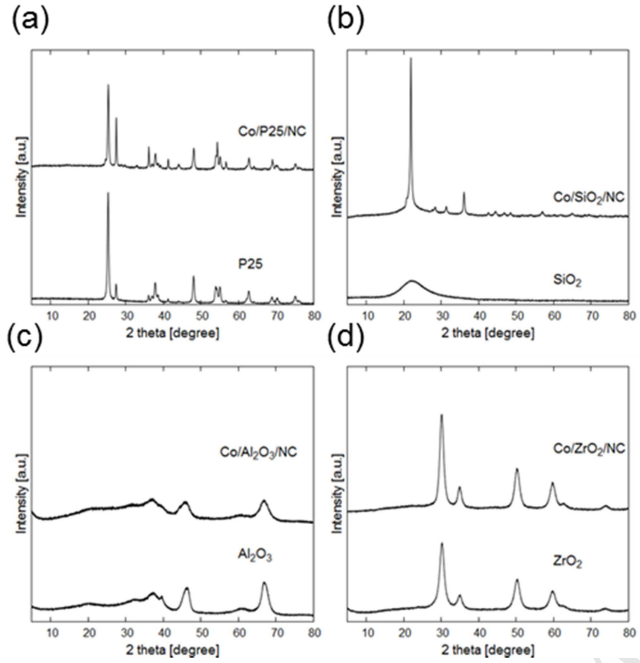

Fig. 1

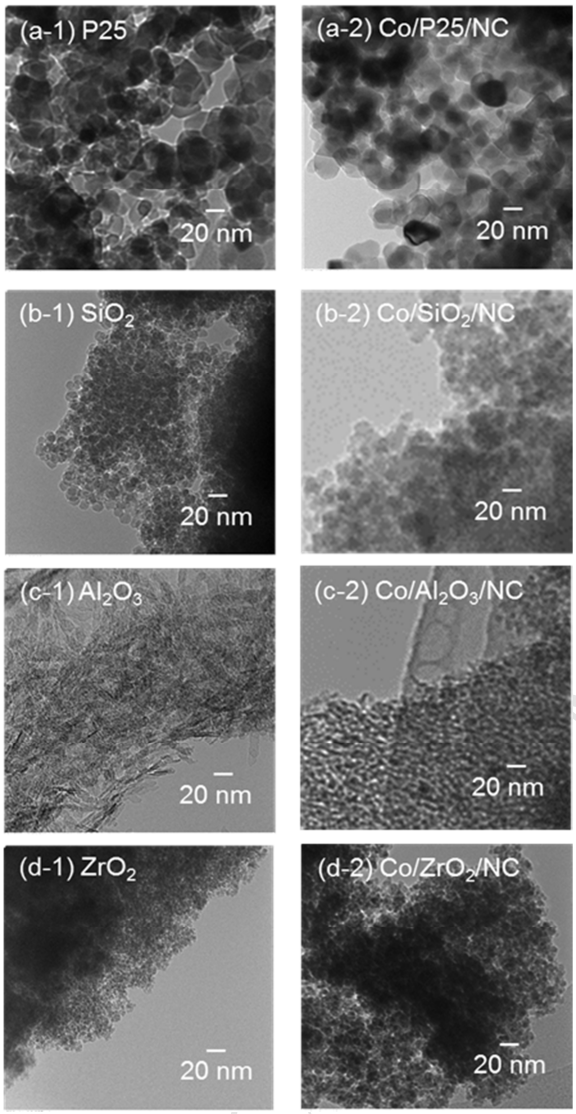

Fig. 2

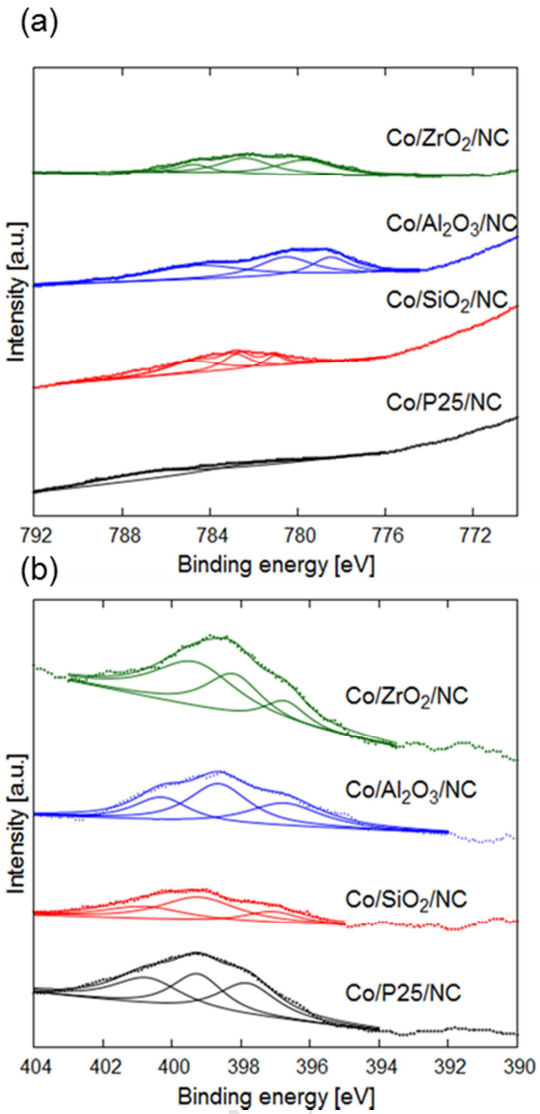

Fig. 3

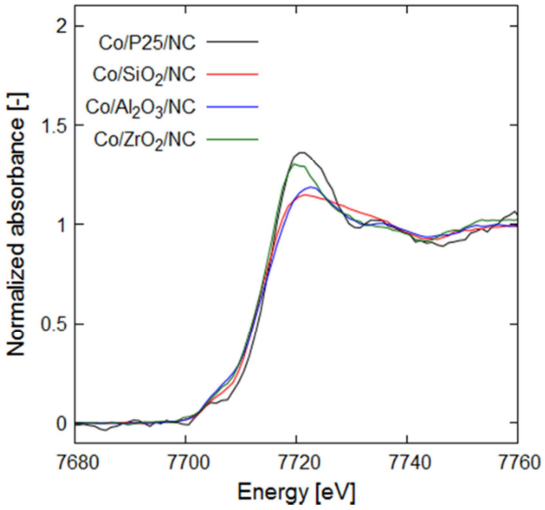

Fig.4

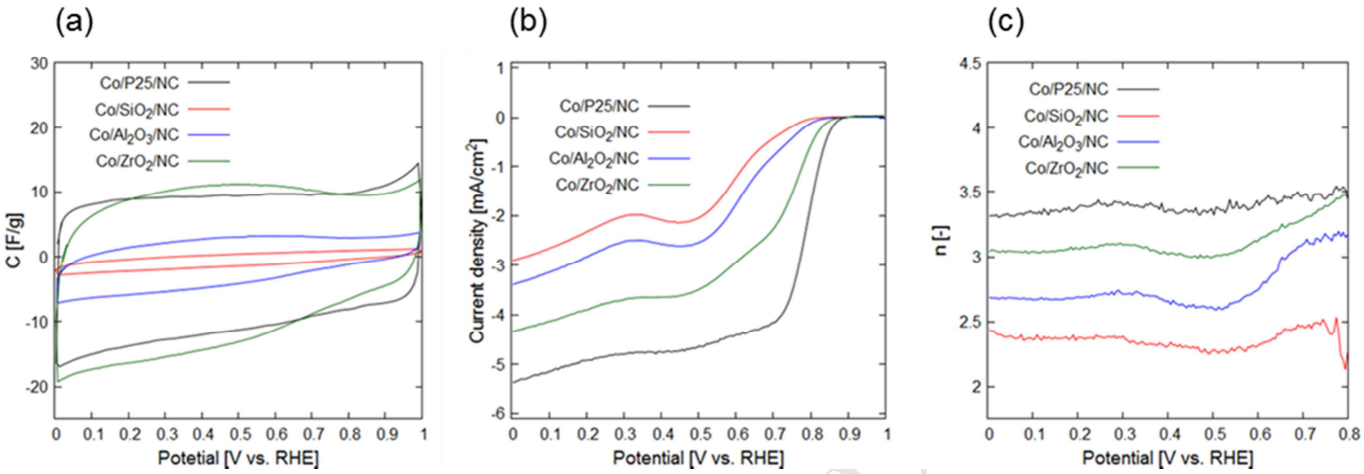

Fig. 5

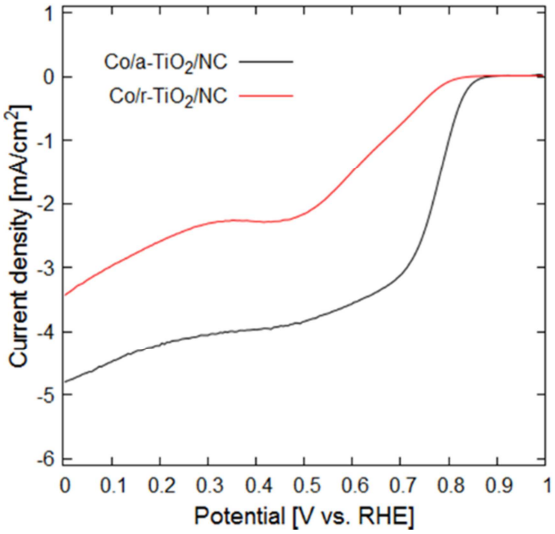

Fig. 6

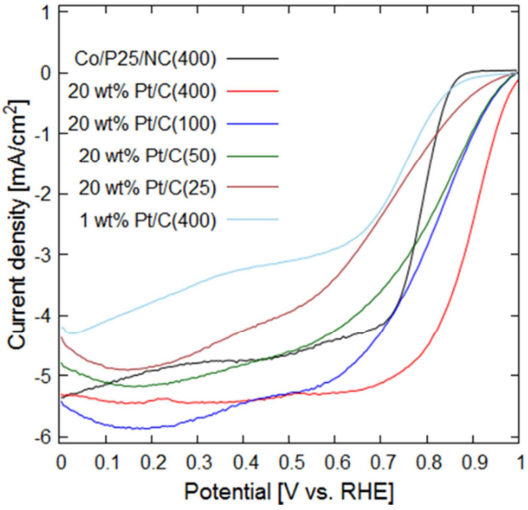

Fig. 7

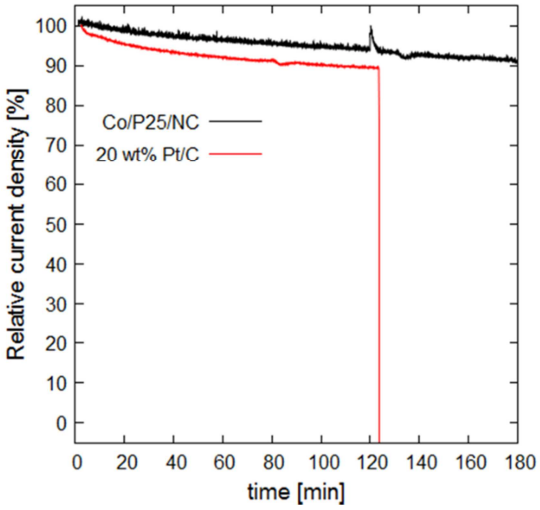

Fig. 8

Table 1

catalysts	Amount of Co or Pt on the disk [μg/cm^2]	Current density @ 0.65V vs. RHE [mA/cm^2]
Co/P25/NC	3	4.31
20 wt% Pt/C	5	2.94
	10	3.98
	20	4.73
	80	5.24
1 wt% Pt/C	4	2.71